1535. Non-linear behavior of a Z-source DC/DC converter based on dual-loop control

Yan Chen[1]**, Yong Zheng**[2]
[1]School of Electronic Information and Automation, Chongqing University of Technology, Chongqing, 400054, China
[2]Chongqing Key Laboratory of Time Grating Sensing and Advanced Testing Technology, Chongqing University of Technology, Chongqing, 400054, China
[2]Corresponding author
E-mail: [1]*chenyan2012@cqut.edu.cn*, [2]*sdzzzy@cqut.edu.cn*

(Received 7 December 2013; received in revised form 16 August 2014; accepted 22 August 2014)

Abstract. As a new topology, Z-source converter can be potentially applied in emerging energy power fields. In contrast to traditional converters, Z-source converter under dual-loop control exhibits particularity, but this property has been rarely investigated. In this study, the bifurcation and chaos phenomena are investigated in the Z-source converter under dual-loop control. A dynamic model with a shoot-through state of the Z-source converter is initially derived. The stability of fixed points is then investigated. The parameter region of a steady-state operation is subsequently schemed. The evolution and mechanism of bifurcations and chaos are also analyzed in detail. Results show that the system is intermittently stable at relatively low V_{ref}, as V_{ref} gradually increases, the system enters a bifurcation state and then exhibits chaos.

Keywords: Z-source converter, non-linear, stroboscopic mapping model, chaos.

1. Introduction

As a new type of power converter, a Z-source converter, which can achieve single-stage buck/boost conversion, has been developed [1]; this converter can be potentially applied in the field of new-generation energy because of its wide input voltage range [2-3]. For instance, the Z-source converter switches periodically under the influence of a control system, causing changes in system topology periodically; the voltage and current of a system then change between different stable points. Each kind of topology corresponds to a linear system, but this system is generally a piecewise non-linear system. This characteristic results in a complex nonlinear dynamics behavior of physical quantities, such as bifurcation and chao of a system. These phenomena adverselyaffect the work performance of a system, particularly the critical state of sudden collapse, electromagnetic noise, unknown instability. Thesephenomena are external manifestations of the inherent non-linear behavior of a Z-source converter [4]. A converter functions in a chaotic state and likely results in an unpredicted and uncontrolled system; as such, the performance of this converter is affected seriously. In some cases, a converter is completely unable to function. This condition causes great difficulty in the design and control of a system. Therefore, non-linear dynamics theory can be applied to analyze and understand the non-linear process and characteristics of a system. In this way, engineering practice can be effectively performed.

These complex non-linear phenomena in power electronic systems have prompted many scholars to perform several studies. In the past 20 years, many studies were conducted on the theory of non-linear dynamics, numerical simulation, and circuit experiment to analyze bifurcation and chaos in this kind of systems. These studies have observed quasi-periodic bifurcation, period doubling bifurcation, border collision bifurcation, intermittent bifurcation, chaos, and other non-linear phenomena [5-8] in a DC/DC converter [9-11], DC/AC inverter [12-13] and power factor correction converter (PFC) [14]. Another example is the Z-source converter that exhibits a unique shoot-through stateand achieves single-state buck-boost converting. The non-linear behavior of this converter is more complex than that of traditional inverters. In anotherstudy, the bifurcation and chaos of a Z-source converter under peak-current control (single-loop) [15]. However, dual-loop control can achieve multi-object control simulaneously; as such, dual-loop control has been widely used. In the present study, a Z-source converter under dual-loop control was used as our object, on the basis of the equation of state, the non-linear behavior of the Z-source converter was modeled using a stroboscopic map method, simulated and analyzedto determine the bifurcation and chaos.

2. Principle of Z-source DC/DC converter

Fig. 1 illustrates the circuit diagram of a Z-source DC/DC converter based on current-mode dual-loop control.

In Fig. 1, a two-port network consisting of the split inductors L_1 and L_2 and the capacitors C_1 and C_2 connected in an X shape manner is used, to analyze this diagram, we assume that $L_1 = L_2 = L$ and $C_1 = C_2 = C$.

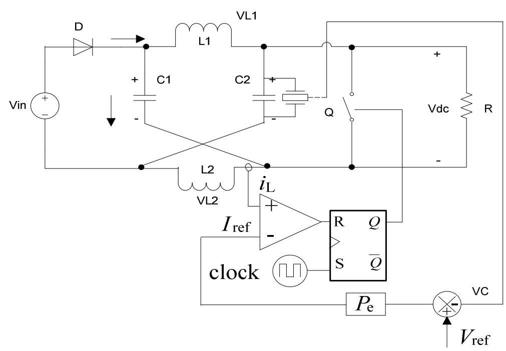

Fig. 1. Schematic of the Z-source DC/DC converter based on current-mode dual-loop control

The schematic of a Z-source DC/DC converter based on dual-loop control is shown in Fig. 1, where V_{in} is the input voltage, V_{ref} is the reference voltage, and P_e is the error gain of the output voltage. This system mainly involves a clock signal that controls the turn-on switch. This clock signal also sets the RS flip-flop to 1 at regular intervals. At $Q = 0$, the switch is turn-off, and the inductor current i_L increases until the required I_{ref} is reached. Afterward, the inductor inverts the output signal of the at $Q = 1$. The current reference I_{ref} is produced by amplifying the error between V_{ref} and the actual output voltage. Current-mode dual-loop control can be performed easily and limits the peak current to protect device; therefore, this system can be used in several applications.

On the basis of the shoot-through switch Q states and the diode D states, we can obtain the two working modes (Fig. 2).

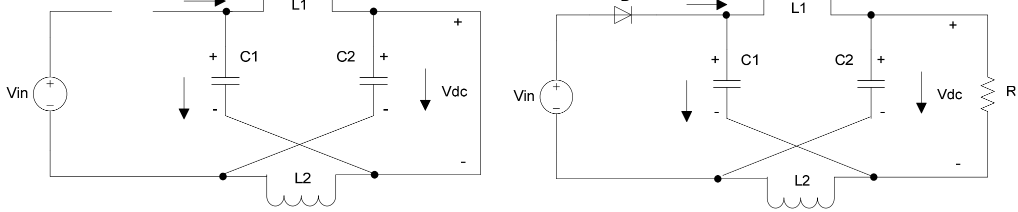

a) Equivalent circuit in shoot-through mode b) Equivalent circuit in non-shoot-through mode

Fig. 2. DC-link equivalent circuit of the Z-source converter

In working mode 1, the shoot-through state is represented as Q on and D off; the state equation is written as follows:

$$\begin{cases} \dfrac{di_L}{dt} = -\dfrac{r_1 + R_1}{L} \cdot i_L + \dfrac{u_c}{L}, \\ \dfrac{du_c}{dt} = -\dfrac{i_L}{C}. \end{cases} \tag{1}$$

In working mode 2, the non-shoot-through state is represented as D off and Q on; the state equation is expressed as follows:

$$\begin{cases} \dfrac{di_L}{dt} = -\dfrac{r_1 + R_1}{L} \cdot i_L + \left(\dfrac{R_1}{RL} - \dfrac{1}{L}\right) \cdot u_c + \dfrac{V_{in}}{L}, \\ \dfrac{du_c}{dt} = \dfrac{i_L}{C} - \dfrac{2u_c - V_{in}}{RC}. \end{cases} \tag{2}$$

The state equation derived from Eqs. (1) and (2) is specified as Eq. (3) and Eq. (4), respectively:

$$\dot{x} = A_1 x + B_1 V_{in}, \;\; nT + t_n \leq t < nT + d_n T, \tag{3}$$
$$\dot{x} = A_2 x + B_2 V_{in}, \;\; nT + d_n T \leq t < (n+1)T, \tag{4}$$

where the state vector $\dot{x}$ is defined as $x = \begin{bmatrix} i_L \\ u_c \end{bmatrix}$, i_L is the inductor current of the Z-source network, u_c is the capacitance voltage of the Z-source network, r_1 is resistor parasitics of the inductor, R_1 is the series resistance of capacitance, R is the load resistance, and V_{dc} is the output voltage:

$$A_1 = \begin{bmatrix} -(r_1 + R_1)/L & 1/L \\ -1/C & 0 \end{bmatrix}, \;\; A_2 = \begin{bmatrix} -(r_1 + R_1)/L & -R_1/L/R - 1/L \\ 1/C & -2/R/C \end{bmatrix},$$
$$B_1 = 0, \;\; B_2 = \begin{bmatrix} 1/L \\ 1/C/R \end{bmatrix}.$$

3. Simulation of the non-linear behavior of a Z-source DC/DC converter

The simulation results (Figs. 3-5) showed that U_c is the capacitance voltage of the Z-source network and i_L is the inductor current of the Z-source network. These figures show the typical waveforms of period-1 state, period-2 state, and chaotic state.

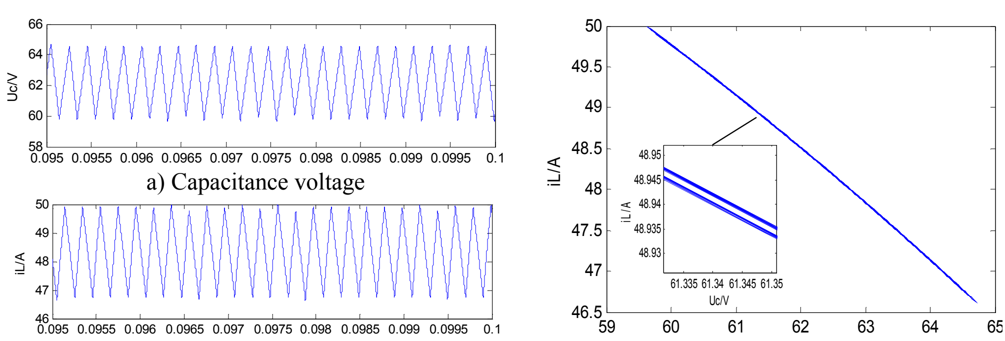

a) Capacitance voltage

b) Inductor current

c) Phase-plane diagram

Fig. 3. Typical waveforms of period-1 state

4. Dynamic modeling and analysis of a Z-source DC/DC converter

4.1. Stroboscopic mapping model

d_n is the duty cycle of the nth period T, where $t_n = nT$, $x_n = x(nT)$; other discrete parameters are defined by similar logic in which the state Eq. (3) and Eq. (4) as well as the discrete model Eq. (6) and Eq. (7) in the nth period are calculated. The discrete mapping equation can be expressed as follows:

$$x_{n+1} = f(x_n, d_n), \tag{5}$$

$$\begin{aligned} x(t_n + d_nT) &= \phi_1(d_nT)x(t_n) + \int_{t_n}^{t_n+d_nT} \phi_1(t_n + d_nT - \tau)\, B_1V_{in}d\tau \\ &= \phi_1(d_nT)x(t_n), \ \ (nT + t_n \leq t < nT + d_nT), \end{aligned} \tag{6}$$

$$\begin{aligned} x(t_{n+1}) &= \phi_2(\bar{d}_nT)x(t_n + d_nT) + \int_{t_n+d_nT}^{t_n+T} \phi_2(t_n + T - \tau)\, B_2V_{in}d\tau \\ &= \phi_2(\bar{d}_nT)x(t_n + d_nT) + \int_0^{\bar{d}_nT} \phi_2(\bar{d}_nT - \tau)\, B_2V_{in}d\tau, \ \ (nT + d_nT \leq t < (n+1)T), \end{aligned} \tag{7}$$

where $\phi_1(d_nT) = e^{A_1d_nT}$, $\phi_2(\bar{d}_nT) = e^{A_2\bar{d}_nT}$, $\bar{d}_n = 1 - d_n$.

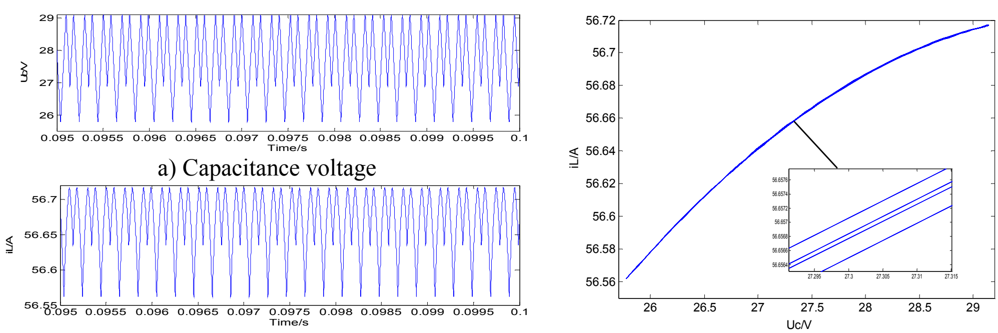

a) Capacitance voltage

b) Inductor current

c) Phase-plane diagram

Fig. 4. Typical waveforms of period-2 state

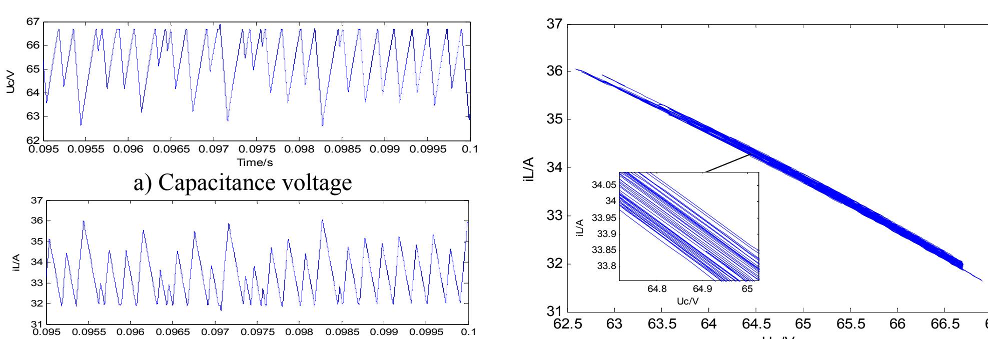

a) Capacitance voltage

b) Inductor current

c) Phase-plane diagram

Fig. 5. Typical waveforms of choatic state

A_1 and A_2 are both invertible matrixes; as a result the integral terms of these equations can be simplified and expressed as follows:

$$x(t_n + d_nT) = \phi_1(d_nT)x_n, \tag{8}$$

$$x(t_{n+1}) = \phi_2(\bar{d}_nT)x(t_n + d_nT) + A_2^{-1}(\phi_2(\bar{d}_nT) - I)B_2V_{in}. \tag{9}$$

Eq. (8) can be substituted in Eq. (9) and expressed as the discrete mapping Eq. (10):

$$x_{n+1} = f(x_n, d_n) = \phi_2(\bar{d}_nT)\phi_1(d_nT)x_n + A_2^{-1}(\phi_2(\bar{d}_nT) - I)B_2V_{in}. \tag{10}$$

The switching function can be derived as follows:

$$\begin{aligned}\sigma(x_n, d_n) &= i_L - \left(V_{ref} - u_c\right) \cdot Pe = k_1 x(t_n + d_n T) - \left[V_{ref} - k_2 x(t_n + d_n T)\right] \cdot Pe \\ &= k_1 \phi_1(d_n T) x_n - \left[V_{ref} - k_2 \phi_1(d_n T) x_n\right] \cdot Pe,\end{aligned} \tag{11}$$

where $k_1 = [1, 0]$, $k_2 = [0, 1]$, and $Pe = 100$ at $\sigma(x_n, d_n) = 0$; as a result, the state of the converter is altered.

Eq. (10) and Eq. (11) can be simultaneously calculated as a non-linear discrete mapping equation of a Z-source converter.

4.2. Stability analysis based on Jacobian matrix method

As a result of changes in the circuit parameter of a system and the effect of external factors, the system likely operates from a stable working mode to unstable working mode. Jacobian matrix method is used to analyze the local bifurcation in the non-linear dynamics system. We can then establish the Jacobian matrix based on a fixed point.

Assuming that the controlled system is stabilized at one-cycle state, and make the input voltage and reference voltage keep constant, let $x_n = \hat{x} + X_Q$, $d_n = \hat{d} + D$, X_Q and D are the stationary solutions.

The perturbation and linearization of Eq. (5) are then expressed as follows:

$$\hat{x}_{n+1} = \frac{\partial f}{\partial x_n} \hat{x}_n + \frac{\partial f}{\partial d_n} \hat{d}_n. \tag{12}$$

At $\sigma(x_n, d_n) = 0$, Eq. (13) is obtained:

$$\frac{\partial \sigma}{\partial x_n} \hat{x}_n + \frac{\partial \sigma}{\partial d_n} \hat{d}_n = 0. \tag{13}$$

Therefore, we can derive Eq. (14) expressed as follows:

$$\hat{d}_n = \left(-\frac{\partial \sigma}{\partial d_n}\right)^{-1} \frac{\partial \sigma}{\partial x_n} \hat{x}_n . \tag{14}$$

Eq. (14) can be substituted to Eq. (12) toobtain Eq. (15):

$$\hat{x}_{n+1} = \left(\frac{\partial f}{\partial x_n} + \frac{\partial f}{\partial d_n}\left(-\frac{\partial \sigma}{\partial d_n}\right)^{-1} \frac{\partial \sigma}{\partial x_n}\right) \hat{x}_n. \tag{15}$$

We can then obtain the Jacobian matrix:

$$J(X_Q) = \frac{\partial f}{\partial x_n} - \frac{\partial f}{\partial d_n}\left(\frac{\partial \sigma}{\partial d_n}\right)^{-1} \frac{\partial \sigma}{\partial x_n}\bigg|_{(X_Q, D)}, \tag{16}$$

where:

$$\frac{\partial \sigma}{\partial x_n} = (k_1 + k_2 \cdot Pe) \cdot e^{A_1 d_n T}, \quad \frac{\partial \sigma}{\partial d_n} = (k_1 + k_2 \cdot Pe) \cdot A_1 T e^{A_1 d_n T} x_n,$$
$$\frac{\partial f}{\partial x_n} = e^{A_2 (1 - d_n) T} e^{A_1 d_n T},$$

$$\frac{\partial f}{\partial d_n} = -TA_2 e^{A_2(1-d_n)T} \cdot e^{A_1 d_n T} x_n + e^{A_2(1-d_n)T} \cdot A_1 T e^{A_1 d_n T} x_n - T e^{A_2(1-d_n)T} B_2 V_{in}.$$

We can set the eigenvalue of Jacobian matrix to λ. According to the system stability, the system is stable when λ is located in the unit circle of a complex plane. Stability is observed when the Jacobian matrix corresponds to the disturbance ratio of two successive iterations (the latter term to the former term). At ratio > 1, the disturbance of the system increases; thus, the system is likely unstable by increasing the iteration number. At ratio < 1, the system is stable. Therefore, the system is likely unstable as the reference voltage is altered.

The periodic solutions X_Q and D are calculated before the eigenvalue of the Jacobian matrix is obtained. The following solutions are used:

Let $x_{n+1} = x_n = X_Q$, $x(nT + d_n T) = X_D$, and $d_n = D$ in Eq. (8) and Eq. (9) to obtain the following equations:

$$X_D = \phi_1 X_Q, \tag{17}$$
$$X_Q = \phi_2 X_D + (\phi_2 - I) A_2^{-1} B_2 V_{in}. \tag{18}$$

Eq. (19) and Eq. (20) are then derived:

$$X_Q = (I - \phi_1\phi_2)^{-1}\left[{A_2}^{-1}(\phi_2 - I) B_2 V_{in}\right], \tag{19}$$
$$X_D = \phi_1 (I - \phi_1\phi_2)^{-1}\left[{A_2}^{-1}(\phi_2 - I) B_2 V_{in}\right]. \tag{20}$$

The switching function satisfies Eq. (21):

$$\sigma(x_n, d_n) = k_1 X_D - (V_{ref} - k_2 X_D) \cdot Pe = 0. \tag{21}$$

Eq. (19) and Eq. (21) can be simultaneously calculated to obtain the stable periodic solutions X_Q and D; the eigenvalue of the Jacobian matrix can then be obtained to determine the stability of the system.

5. Numerical simulation and result analysis

Our simulation is based on the state equations derived in Section 4. We investigated the dynamics of the state variable by using V_{ref} as a bifurcation parameter. The circuit parameters used in our simulation are listed as follows: $C_1 = C_2 = C = 1{,}000$ μF, $L_1 = L_2 = L = 1$ mH, $V_{in} = 60$ V, $R = 6\ \Omega$, $R_1 = 0.03\ \Omega$, $r_1 = 0.5\ \Omega$, and $f = 10$ kHz. We obtained a bifurcation diagram (Fig. 6). Fig. 6 summarizes u_c at the beginning of each switching period as V_{ref} increases.

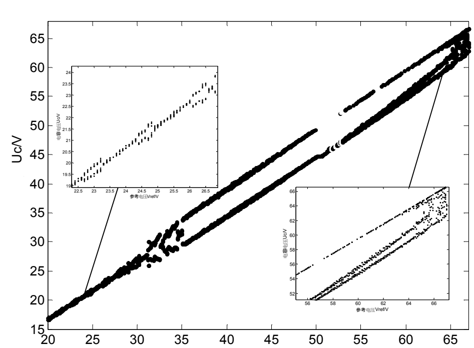

Fig. 6. Bifurcation diagram of u_c

Fig. 6 also shows that the system exhibits a period-1 orbit at relatively low V_{ref}. This orbit indicates that the system is stable. This orbit should also be stabilized at a widened range. In the Z-source converter under dual-loop control, the period-1 orbit is intermittent which observed from the partially enlarged detail. As V_{ref} increases, the period-2 orbit is observed, and the branch point is approximately $V_{ref} = 30$ V. As V_{ref} increases, chaos occurs. Therefore, Fig. 6 illustrates the path from stability to chaos.

Fig. 7 shows the effect of variations in V_{ref} on the stability of the Z-source converter. The system is initially stable, and the twoJacobian matrixeigenvalues are mapped in the unit circle. As V_{ref} is gradually increased, one of the eigenvalues leaves the unit circle. This result indicates a period-2 bifurcation, rapidly results in instability and chaos. The eigenvalues are listed in Table 1.

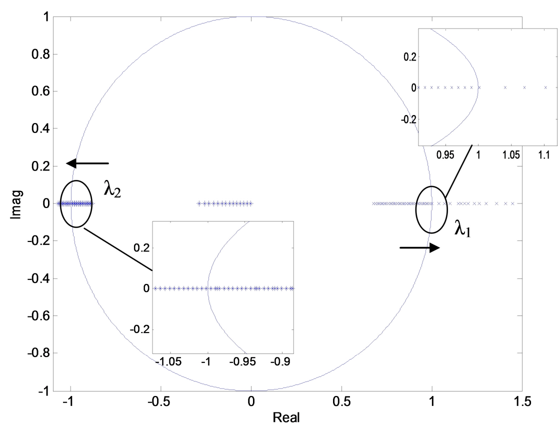

Fig. 7. Movement of eigenvalues for a dual-loop controlled Z-source converter

Table 1. Eigenvalues of different values of the reference voltage V_{ref} for dual-loop control

V_{ref}	D	λ_1	λ_2	System state	V_{ref}	D	λ_1	λ_2	System state
23	0.4792	0.8084	-0.9604	stable	38	0.4979	0.9291	-1.0323	unstable
24	0.4809	0.8184	-0.9663	stable	42	0.5008	0.9493	-1.0447	unstable
25	0.4825	0.8284	-0.9722	stable	46	0.5037	0.9696	-1.0573	unstable
26	0.4841	0.8384	-0.9781	stable	48	0.5052	0.9798	-1.0637	unstable
27	0.4857	0.8485	-0.9841	stable	50	0.5066	0.9899	-1.0701	unstable
28	0.4873	0.8585	-0.9900	stable	51	0.5081	1.0020	-0.2879	unstable
29	0.4888	0.8686	-.9960	stable	52	0.5095	1.0409	-0.2602	unstable
30	0.4904	0.8786	-1.0020	bifurcation	53	0.5109	1.0707	-0.2344	unstable
31	0.4919	0.8887	-1.0080	unstable	54	0.5124	1.1028	-0.2099	unstable
32	0.4934	0.8988	-1.0140	unstable	55	0.5138	1.1466	-0.1865	unstable
34	0.4949	0.9089	-1.0201	unstable	57	0.5166	1.1804	-0.1422	unstable

Table 1 shows that $|\lambda_1|$ is approximately equal to 1 at $V_{ref} = 30$ V. On the basis of numberical calculations, we can obtain the following: at values exceeding $V_{ref} = 30$ V, $\lambda_1 = 0.8786$, and $\lambda_2 = -1.0020$, where V_{ref} is the critical value of the unstable system, the system experiences a bifurcated and chaotic state. At $V_{ref} < 30$ V, eigenvalues < 1; as V_{ref} increases, $|\lambda_1|$ moves toward –1. This result indicates the occurrence of period-2 bifurcation; as V_{ref} continuously increases, $|\lambda_2|$ moves toward 1 at $V_{ref} = 50$ V, which happens jump. The two eigenvalues change along the real axis, and $|\lambda_1|$ changes more rapidly than $|\lambda_2|$. If any of these eigenvalues is > 1, the system becomes unstable.

As the system is controlled in period –1, the boundaries of a stable region or an unstable region are presented in this section. V_{in} and V_{ref} are selected as the variations. The operation boundaries

(Fig. 8) are derived from the analytical solutions and cycle-by-cycle simulation. The two results complement each other. The operation boundary provides essential design-oriented information in which system parameters are selected systematically.

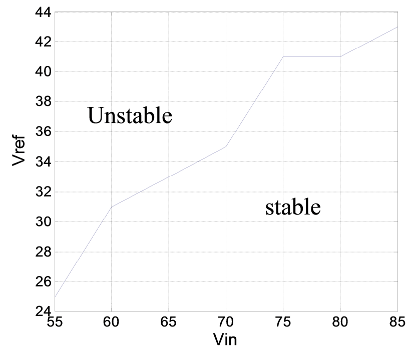

Fig. 8. Stable region boundary with altered parameters

6. Experiment verifications

To verify the theoretical analysis result, we established an experimental circuit prototype of the Z-source converter under dual-loop control (Fig. 9). The main circuit of the Z-source converter is shown in Fig. 9(a) and the control signal is generated using RT-lab equipment [Fig. 9(b)]. All of the parameters are similar to those in Section 4. The experimental waveforms in Fig. 10 are period-1, period-2, and chaos respectively. Fig. 10(a) shows stable period-1 at $V_{ref} = 25$ V, Fig. 10(a) shows the stable period-1 at $V_{ref} = 25$ V. Fig. 10(b) shows the stable period-2 at $V_{ref} = 32$ V. Fig. 10(c) shows the chaos phenomenon. The experimental results are consistent with the theoretical analysis. These results also confirm the correctness of the theoretical analysis. In Fig. 10, the oscilloscope channel-1 displays the Z-source capacitor voltage u_c, and channel-2 shows the Z-source inductance current i_L.

a) Main circuit b) RT-lab controller

Fig. 9. Experimental platform

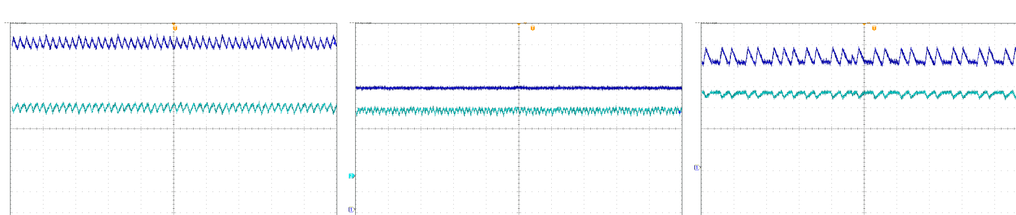

a) Period-1, $V_{ref} = 25$ V b) Period-2, $V_{ref} = 32$ V c) Chaos, $V_{ref} = 67$ V

Fig. 10. Experimental waveform

7. Conclusions

The Z-source converter can be potentially applied in emerging energy technologies and distributed generation. In this study, the Z-source DC/DC converter is used as the object under dual-loop control. The stroboscopic mapping model is established to analyze the non-linear behavior of the converter. Simulations and experimental results are presented for verification purposes. The researchers of this study expanded the non-linear research fields involving converters; the system provides an important theoretical basis and is of practical significance in engineering.

Acknowledgements

This study is supported by the Basic and Frontier Research Program of Chongqing Municipality (Grant No. cstc2013jcyjA0531) and the Science and Technology Special Foundation of Banan District of Chongqing (Grant No. 2012Q120).

References

[1] **Peng Fangzheng** Z-source inverter. IEEE Transactions on Industry Applications, Vol. 39, Issue 2, 2003, p. 504-510.

[2] **Baoming Ge, Abu-Rub H., Peng Fangzheng, et al.** An energy-stored quasi-Z-Source inverter for application to photovoltaic power system. IEEE Transactions on Industrial Electronics, Vol. 60, Issue 10, 2013, p. 4468-4481.

[3] **Dehghan S. M., Mohamadian M., Varjani A. Y.** A new variable-speed wind energy conversion system using permanent-magnet synchronous generator and Z-Source Inverter. IEEE Transactions on Energy Conversion, Vol. 24, Issue 3, 2009, p. 714-724.

[4] **Zhang Bo** Study of nonlinear chaotic phenomena of power converters and their applications. Transactions of China Electrotechnical Society, Vol. 20, Issue 12, 2005, p. 1-6.

[5] **Zhusubaliyev Zhanybai T., Soukhoterin E. A., Mosekilde E.** Quasi-periodicity and border-collision bifurcations in a DC-DC converter with pulsewidth modulation. IEEE Transactions on Circuits and Systems I: Fundamental Theory and Applications, Vol. 50, Issue 8, 2003, p. 1047-1057.

[6] **Dai Dong, Ma Xikui, Li Xiaofeng** Border collisionbifurcations and chaos in a class of piecewise smoothsystems with two boundaries. Acta Physica Sinica, Vol. 52, Issue 11, 2003, p. 2729-2736.

[7] **Zhang Hao, Ma Xi-kui, XueBian-ling, Liu Wei-zeng** Study of intermittent bifurcations and chaos in boost. Chaos, Solitons and Fractals, Vol. 23, 2005, p. 431-444.

[8] **Xie Fan, Yang Ru, Zhang Bo** Bifurcation and border collision analysis of voltage-mode-controlled flyback converter based on total ampere-turns. IEEE Transactions on Circuits and Systems I: Regular Papers, Vol. 58, Issue 9, 2011, p. 2269-2280.

[9] **Premalatha L., Vanaja Ranjan P.** Spectral analysis of DC-DC buck converter with chaotic dynamics. Annual IEEE INDICON, 2005, p. 605-608.

[10] **Basak B., Parui S.** Exploration of bifurcation and chaos in buck converter supplied from a rectifier. IEEE Transactions on Power Electronics, Vol. 25, Issue 6, 2010, p. 1556-1564.

[11] **Deivasundari P., Uma G., Poovizhi R.** Analysis and experimental verification of Hopf bifurcation in a solar photovoltaic powered hysteresis current-controlled cascaded-boost converter. IET Power Electronics, Vol. 6, Issue 4, 2013, p. 763-773.

[12] **Fei-Hu Hsieh, Hen-Kung Wang, Po-Lun Chang, Hsuan-Chiang Wu** Nonlinear dynamic behaviors in voltage-mode controlled single-phase half-bridge inverters via varying proportional gain. International Conference on Machine Learning and Cybernetics, 2011, p. 1274-1278.

[13] **Iu H. H. C., Robert B.** Control of chaos in a PWM current-mode H-bridge inverter using time-delayed feedback. IEEE Transactions on Circuits and Systems I: Fundamental Theory and Applications, Vol. 50, Issue 8, 2003, p. 1125-1129.

[14] **Meng Huang, Tse C. K., Siu-Chung Wong, Cheng Wan, Xinbo Ruan** Low-frequency Hopf bifurcation and its effects on stability margin in three-phase PFC power supplies connected to non-ideal power grid. IEEE Transactions on Circuits and Systems I: Regular Papers, Vol. 60, Issue 12, 2013, p. 3328-3340.

[15] **Chen Yan, Zheng Yong** Nonlinear behavior analysis of Z-source DC/DC converter based on current control. Journal of Vibroengineering, Vol. 15, Issue 3, 2013, p. 1576-1584.

Yan Chen received the BS degree in Electronics Information Engineering from Air Force Engineering University, China, in 2005, received the MS degree in Testing and Measurement Technology and Instrument from Chongqing University of Technology, China, in 2008, and her Ph.D. degrees in Electrical Engineering from Chongqing University, China, in 2012. She is a Lecturer in College of Electronic Information and Automation, Chongqing University of Technology. Her research interests include power electronic devices and systems and nonlinear control technology.

Yong Zheng received the BS degree in Mechanical Engineering and Automation from Qingdao University of Science and Technology, China, in 2005, received the MS and PhD degree in Measurement Technology and Instrumentation from Chongqing University of Technology, China, in 2008 and Hefei University of Technology, China, in 2011, respectively. Presently he is an assistant researcher at the Engineering Research Center of Mechanical Testing Technology and Equipment, Ministry of Education in Chongqing University of Technology, and he is particularly interested in mechanical detection and control.